Thermal transport in novel carbon allotropes with sp^2 or sp^3 hybridization: An *ab initio* study

Sheng-Ying Yue,[1] Guangzhao Qin,[2] Xiaoliang Zhang,[2] Xianlei Sheng,[3] Gang Su,[4,*] and Ming Hu[1,2,†]

[1]*Aachen Institute for Advanced Study in Computational Engineering Science (AICES), RWTH Aachen University, 52062 Aachen, Germany*

[2]*Institute of Mineral Engineering, Division of Materials Science and Engineering, Faculty of Georesources and Materials Engineering, RWTH Aachen University, 52064 Aachen, Germany*

[3]*Department of Applied Physics, Beihang University, Beijing 100191, China*

[4]*Kavli Institute for Theoretical Sciences, and School of Physics, University of Chinese Academy of Sciences, P. O. Box 4588, Beijing 100049, China*

(Received 16 December 2016; revised manuscript received 6 February 2017; published 27 February 2017)

Thermal transport in most carbon allotropes is determined by phonons. The properties of the atomic bonds will influence the phonon transport process directly. In this paper we studied two novel carbon allotropes as examples, one novel allotrope phase is topological semimetal in an sp^2 bonding network with a 16-atom body-centered orthorhombic unit cell (BCO-C_{16}) [Phys. Rev. Lett. **116**, 195501 (2016)] and the other novel allotrope is derived by substituting each atom in diamond with a carbon tetrahedron (T-carbon) [Phys. Rev. Lett. **106**, 155703 (2011)], which possesses an sp^3 bonding network. Graphene and diamond with standard sp^2 and sp^3 hybridization, respectively, are also examined for comparison. We explored the related properties of the atomic bonds of these allotropes with the density functional theory, i.e., the atomic orbital hybridization, effective spring constants of atomic bonds, the anharmonicity of atomic bonds, etc. By comparing the results, we unveiled the veil behind different lattice thermal conductivities of these allotropes at atomic bond levels (BCO-C_{16} vs graphene and T-carbon vs diamond), despite their similar hybridization. In addition, within the framework of a phonon Boltzmann transport equation, the mode level phonon transport properties of the four carbon allotropes are also studied in detail, which are well consistent with the information from atomic bonds. We expect that the method of analyzing the strength and anharmonicity of atomic bonds here will be helpful for studying the thermal transport in crystalline materials in the future.

DOI: 10.1103/PhysRevB.95.085207

I. INTRODUCTION

Thermal transport, mainly lattice thermal conductivity (κ), is crucial for enormous practical implications, such as heat dissipation in electronics and heat hindering in thermoelectrics. Phonon anharmonicity is a critical factor to determine κ. In principle, phonon anharmonicity is determined by the phonon scattering, which is further related to three-phonon and higher-order phonon interactions. For most crystals the higher-order phonon interactions can be ignored in determining κ. In this framework, the anharmonic lattice dynamics (ALD) method coupled with the phonon Boltzmann transport equation (BTE) is one of the most featured methods to obtain κ. With the help of the ALD/BTE method, understanding of phonon anharmonicity is extended to the anharmonic interatomic force constants, mainly the so-called third-order derivatives of potential energy with respect to atomic displacement, along with the mode level phonon behaviors such as phonon lifetime, scattering channel, etc. Considering all the interatomic interactions should be intrinsically related to the form of atomic orbitals and orbital hybridization, which are determined by the atomic structure, it is interesting to look at how the atomic orbitals influence the phonon transport at the level of atomic bonds.

Carbon-based materials play a very important role in modern science and technology. Especially some pure allotropes of carbon own very unique properties. For example, the charge carriers in two-dimensional (2D) graphene mimic relativistic particles with zero rest mass and have an amazing speed $c^* \approx 10^6$ m/s [1]. Diamond is the hardest known natural material [2]. The high density of strong carbon-carbon bonds in diamond and the three-dimensional arrangement of such bonds account for the hardness of diamond [2]. With the development of synthesis technology, various pure forms of carbon allotropes are successfully synthesized, i.e., fullerenes [3], nanotubes [4], and graphene [5]. These synthesized allotropes give rise to enormous impacts in science of chemistry, physics, and materials, and lead to the revolution of nanotechnology and nanodevices. Meanwhile, with the improvement of density functional theory (DFT), scientists have the opportunity to predict novel carbon allotropes and study the related fascinating physical and chemical properties.

In this paper, resorting to first-principles calculations, we study the thermal transport in two novel three-dimensional (3D) carbon allotropes. The first phase is a full sp^2 carbon allotrope with $Imma$ symmetry proposed recently [6]. This phase has a 16-atom body-centered orthorhombic unit cell, termed "BCO-C_{16}", which can be regarded as 3D modification of graphite, consisting of benzene linear chains connected by ethene-type planar π conjugation. The previous study shows that BCO-C_{16} belongs to a new class of topological node-line semimetals, which exhibits novel electronic and transport properties [6]. The other phase is a full sp^3 carbon allotrope in the same symmetry of $Fd\bar{3}m$ as diamond [7]. This phase can be obtained by substituting each atom in diamond by a carbon tetrahedron, termed "T-carbon". It was shown that T-carbon has a low density of 1.50 g/cm^3 and is a semiconductor with a direct band gap of about 3.0 eV, which could be potentially used for hydrogen storage, adsorption,

*gsu@ucas.ac.cn
†hum@ghi.rwth-aachen.de

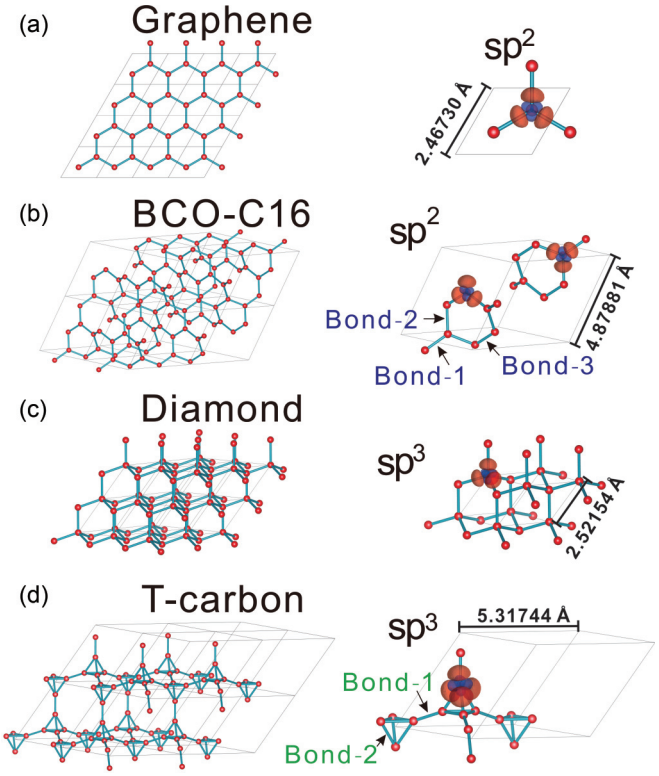

FIG. 1. (Left panels) The models and the primitive cells of (a) graphene, (b) BCO-C_{16}, (c) diamond, and (d) T-carbon. (Right panels) The corresponding hybrid orbitals plotted on the primitive cells. The bond index are shown for BCO-C_{16} and T-carbon in (b) and (d), respectively.

and aerospace materials [7]. For comparison we also study the thermal transport in graphene and diamond. The study on heat transfer properties of these carbon allotropes can help us understand the thermodynamic mechanism of the carbon based materials from an atomic orbital perspective, which is significant to the field of nanodevice design. The remainder of the paper is organized as follows. In Sec. II a brief description about our first-principle calculation is given. In Sec. III we present our main results. First, we use the tight-binding model to investigate the energy of bonds in each model. Second, with the *ab initio* calculations, we analyze the strengths and anharmonicity of the different hybrid bonds in detail. Then we present the key parameters of the phonon transport to establish the relationship between the hybrid bonding style and the thermal conductivity. Finally, our concluding remarks are summarized in Sec. IV.

II. COMPUTATIONAL MODELS AND METHOD

The optimized structures of four allotropes, namely graphene, BCO-C_{16}, diamond, and T-carbon, are shown in the left panel of Fig. 1. The hybrid atomic orbital of a carbon atom in each allotrope is also plotted in the right panel of Fig. 1. The optimized lattice constants of each allotrope unit cell are also presented in Fig. 1. The hybrid atomic orbitals here are calculated from maximally localized Wannier function (MLWF) orbitals [8,9] with the software package Wannier90 [10] and the Vienna *ab initio* simulation package (VASP) [11,12]. From the geometrical structures and symmetry, we can learn that graphene and diamond only own one nonequivalent type of atoms and one unique type of atomic bond, BCO-C_{16} has two nonequivalent types of atoms and three types of atomic bond, and T-carbon owns one nonequivalent type of atoms and two types of atomic bond. The different types of atomic bond of BCO-C_{16} and T-carbon are indexed in Figs. 1(b) and 1(d).

Most of the calculations were performed with the density functional theory (DFT) as implemented within VASP [11,12] with the projector augmented wave (PAW) method [13,14]. The generalized gradient approximation (GGA) was adopted for the exchange-correlation potentials [15] and $2s^2 2p^2$ orbitals are treated as the valence electrons. The plane-wave cutoff energy is 1000 eV. The Monkhorst-Pack scheme was used for sampling the Brillouin zone (BZ). For 3D allotropes BCO-C_{16}, T-carbon, and diamond, the k points sampling meshes are adopted as $8 \times 8 \times 8$, and a mesh of $10 \times 10 \times 1$ is used for 2D graphene. The geometries structures of all allotropes were optimized with the Hellmann-Feynman force tolerance 0.01 eV/Å on ions.

III. RESULTS AND DISCUSSION

A. Thermodynamic stability of carbon allotropes

To identify the thermodynamic stability of these carbon allotropes, we implemented the software package PHONOPY [16] combining with the VASP to calculate the phonon dispersion and phonon density of states (DOS). The results are presented in Fig. 2. The results of phonon dispersions show that there is no imaginary frequency in the entire BZ for all allotropes, confirming the kinetic stability of these structures. From Figs. 2(a) and 2(b) we know that the highest phonon frequency of BCO-C_{16} is located at the X point with the value of ~47.51 THz, which is slightly lower than that of graphene (~47.94 THz). Meanwhile, from Figs. 2(c) and 2(d), we can see that the highest phonon frequency of T-carbon is located at the Γ point with the value of ~54.18 THz, which is higher than that of diamond (~39.29 THz). It is worth to notice that there exists a large gap (10.13 THz) in T-carbon between high frequency optical phonons and middle and low frequency optical phonons (in the range of 22.41–32.54 THz). All of the above results here are consistent with previous studies [6,7].

B. Orbital hybridization

The valence electron configuration of a carbon atom is described as $2s^2 2p^2$, which shows that the carbon atom shares more electrons to achieve the stable noble gas configuration than any other nonmetal atom. The sp^2 and sp^3 hybrid orbitals are the representative hybridizations in pure carbon allotrope. Based on the geometry structures shown in Fig. 1, we formulate the analytical expression of the hybrid orbitals of four allotropes (see the Supplemental Material [17]). We also constructed the atomistic tight-binding (TB) Hamiltonian in maximally localized Wannier function (MLWF) orbitals [8,9], with one s orbital and three p orbitals centered for each carbon atom. We implemented the software package Wannier90 [10] and VASP [11,12] to calculate the interatomic matrix elements between the atomic orbitals m and l on adjacent atoms of the

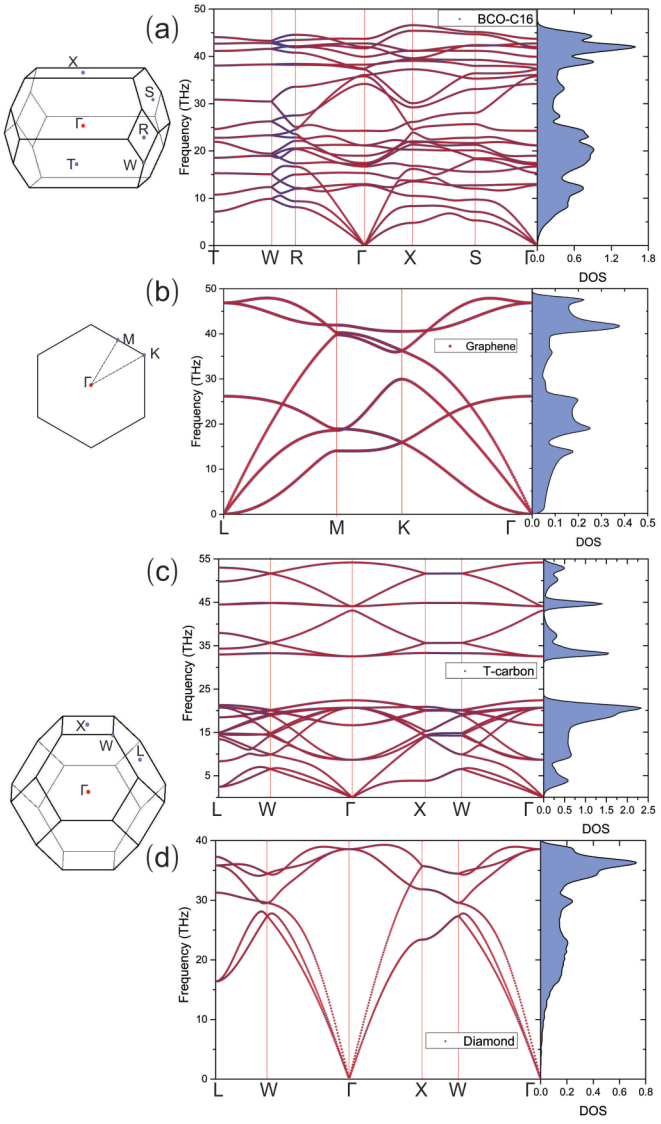

FIG. 2. Phonon dispersion and phonon density of states (DOS) of (a) BCO-C_{16}, (b) graphene, (c) T-carbon, and (d) diamond. The corresponding first Brillouin zones are also shown.

allotropes [10]:

$$\gamma_{m,l}(R_n) = -\int \phi_m^*(r)\Delta U(r)\phi_l(r - R_n)d^3r,$$

which is also called the bond energy or two center integral and is the most important element in the tight-binding model. Here $\phi_m^*(r)$ and $\phi_l(r - R_n)$ are the conjugate of atomic orbital and atomic orbital at position R_n, respectively, and $\Delta U(r)$ is the atomic potential. We can use the interatomic matrix element to indicate the composite interacting energy between the carbon atoms, then further analyze the interactions among the atoms in different carbon allotropes. We consider the adjacent two center approximations ($R_n = 1$) to indicate the bond energy in different models (see the labels of bonds in Fig. 1).

In Table I we present the two center integral $\gamma_{m,l}(R_n)$ in the tight-binding models. The sign before the matrix elements in Table I is just related with direction for the integration in space (i.e., from atom-1 to atom-2 or opposite direction). Thus we can see the matrix elements in Table I are symmetrical along the diagonal, and only the magnitude is significant here. From the matrix of sp^2 in Table I, we can learn that for BCO-C_{16} the two center integrals (also known as overlap integrals) are different from the values of the regular sp^2 present in graphene. This is, because of that, the adjacent four carbon atoms are not exactly in one plane, which leads to the overlap integrals deviating from the standard sp^2 hybridization, as is the case for graphene. This simulating result is different from the mathematical expression of the standard hybrid orbitals (see Supplemental Materials [17]). Because of the inexact plane of carbon atoms in BCO-C_{16}, the orbital hybridization are not pure sp^2. For example, in the hybridization of the bond-2 in BCO-C_{16}, all the p_x, p_y, and p_z participate in the orbital hybridization. In Table I we can also learn that the bond-1 (intertetrahedron) in T-carbon owns the similar overlap integration of standard sp^3 orbitals as in diamond [the diagonal elements beside the $s(m)s(l)$ are almost zero in both T-carbon bond-1 and diamond]. However, the overlap integration of bond-2 (intratetrahedron) in T-carbon are much different from the standard sp^3. This result is consistent with the fact that the T-carbon phase is obtained by substituting each atom in diamond by a carbon tetrahedron.

Then we calculated the summation of the absolute value of the two center integrals in Table I to demonstrate the bonding energy of hybrid orbitals. As the matrix elements are symmetric, we only need to consider the elements of the upper triangular matrix for each allotrope. Because the summation should follow sp^2 or sp^3 hybridizing rules, from the data in Table I, we calculated all possible hybridizations of each bond. For example, for graphene we consider s, p_x, and p_y orbitals; for bond-1 in BCO-C_{16}, the s, p_z, and p_x orbitals most likely participate in the sp^2 hybridization; for bond-3 in BCO-C_{16}, there exist two possible forms for the sp^2 hybridization: one is the hybridization from s, p_z, and p_x orbitals and the other is the s, p_x, and p_y orbital hybridization. For bond-2 in BCO-C_{16}, all overlap integrals among s and p orbitals are not zero, thus we only need to calculate three possible ways for sp^2 hybridization. For the sp^3 hybridizations in Table I, the situation becomes simple: because all the orbitals (s, p_z, p_x, and p_y) participate in the sp^3 hybridization, it is sufficient to consider the elements of the upper triangular matrix in Table I. All possible summations for each bond are presented in Table II, from which we can get the information of the bonding strength of the atomic orbitals for each atomic bond. First, we may see that for sp^2 bonds, all the three bonds of BCO-C_{16} are weaker than those of graphene, especially for the bond-2 in BCO-C_{16}. From the matrix elements in Table I, we find that the BCO-C_{16} bond-2 is the most different from the standard sp^2 hybridization in graphene. Second, for sp^3 bonds the two bonds of T-carbon own the bonding strength of orbitals weaker than diamond. Similar to the results of sp^2 situation, the bond-2 in T-carbon is weaker than bond-1, because the bond-2 is more different from the standard sp^3 hybridization in diamond. It is worth noting that in Table II the standard sp^2 and sp^3 own almost the same largest bonding strength of atomic orbitals.

In addition, the heat transfer process depends on the atomic bonds, which are also intrinsically determined by the atomic orbitals. Generally speaking, the overlap integral can reflect

TABLE I. The interatomic matrix element between the atomic orbitals m and l on the adjacent atoms of the allotropes corresponding to sp^2 and sp^3 bonds in Fig. 5. The unit of the interatomic matrix element is eV.

sp^2 bonds	Orbital m	$s(l)$	$p_z(l)$	$p_x(l)$	$p_y(l)$	sp^3 bonds	Orbital m	$s(l)$	$p_z(l)$	$p_x(l)$	$p_y(l)$
BCO-C_{16}	$s(m)$	−4.0918	−3.7117	−5.4323	−0.0003	T-carbon	$s(m)$	−1.6387	2.9013	−2.9012	−2.9014
	$p_z(m)$	3.7115	0.2571	4.5552	0.0001		$p_z(m)$	−2.9001	0.5683	−3.1188	−3.1189
Bond-1	$p_x(m)$	5.4319	4.5553	3.6385	0.0004	Bond-1	$p_x(m)$	2.9000	−3.1188	0.5680	3.1187
	$p_y(m)$	0.0001	−0.0003	−0.0002	−3.3870		$p_y(m)$	2.9002	−3.1188	3.1187	0.5680
BCO-C_{16}	$s(m)$	−3.2812	1.7130	−2.9370	4.9117	T-carbon	$s(m)$	−1.9693	2.9496	−0.7587	−2.9497
	$p_z(m)$	−1.7030	−1.8315	−1.1717	2.2510		$p_z(m)$	−2.9499	2.3065	0.1260	−4.2473
Bond-2	$p_x(m)$	2.8035	−1.2111	−0.7579	−3.6735	Bond-2	$p_x(m)$	−0.7590	−0.1252	−2.7194	0.1252
	$p_y(m)$	−4.8021	2.0823	−3.7236	3.6599		$p_y(m)$	2.9497	−4.2471	−0.1258	2.3063
BCO-C_{16}	$s(m)$	−4.5989	0.0001	6.7080	0.0002	Diamond	$s(m)$	−3.6094	3.1377	3.1380	3.1376
	$p_z(m)$	0	−2.9628	0	−0.1479		$p_z(m)$	−3.1377	0.3871	2.7730	2.7684
Bond-3	$p_x(m)$	−6.7079	0.0002	6.6074	0.0002		$p_x(m)$	−3.1380	2.7730	0.3891	2.7704
	$p_y(m)$	0	−0.1481	0	−3.4112		$p_y(m)$	−3.1376	2.7684	2.7704	0.3905
Graphene	$s(m)$	−4.9527	0	3.1171	5.4752						
	$p_z(m)$	0	−2.6968	0	0						
	$p_x(m)$	−3.1498	0	−0.6354	4.1469						
	$p_y(m)$	−5.5434	0	4.1868	4.1849						

the bonding strength of the covalent bonds. The two center overlap integrals between adjacent atomic orbitals as shown in Table I may determine the main interactions between the carbon atoms, which further influence the properties of lattice thermal transport. In the rest part of this paper, we will discuss the related properties such as the bond strength and anharmonicity in atomic bonds to verify this point.

To confirm our TB calculations, we also calculate the electronic band structures of each allotrope, which are shown in Fig. 3. The electronic band structures are projected onto the atomic orbitals s, p_x, p_y, and p_z. From Fig. 3(a) we can clearly see the double Dirac-cone structure in BCO-C_{16}, which indicates that BCO-C_{16} is a novel topological semimetal [6]. Meanwhile, from Fig. 3(a), we know that the electronic bands near the Fermi surface are mostly from the p_z orbitals of carbon atoms. Next, from Fig. 3(b), we observe the typical electronic band structure with a single Dirac cone of graphene [1]. Similar to BCO-C_{16} the band of a single Dirac cone is mostly from the p_z electrons. From Figs. 3(a) and 3(b) we can find that for carbon allotropes with sp^2 hybridization, the conducting electrons mostly belong to the hybrid π bond from atomic orbital p_z, and the force interactions among the carbon atoms mostly originate from the σ bonds. Analogously, from Figs. 3(c) and 3(d), we know that the direct energy gaps of T-carbon and diamond are 2.244 and 5.719 eV at the Γ point, respectively, which are consistent with the previous results of 2.25 eV for T-carbon [7] and experimental measurement of 5.45 eV for diamond [18].

TABLE II. The summation of the absolute value of interatomic matrix elements for each kind of bond in Table I following the sp^2 and sp^3 hybridizing rules. The possible ways of summations are presented. Because the interatomic matrix elements are symmetrical along the diagonal in Table I, we consider the elements of the upper triangular matrix for each atomic bond of allotropes.

sp^2 bonds	Sum forms for the absolute values of interatomic matrix elements of sp^2 in Table I	Value (eV)
BCO-C_{16} Bond-1	$\|s(m)s(l)\| + \|s(m)p_z(l)\| + \|s(m)p_x(l)\| + \|p_z(m)p_z(l)\| + \|p_z(m)p_x(l)\| + \|p_x(m)p_x(l)\|$	21.6866
BCO-C_{16} Bond-2	$\|s(m)s(l)\| + \|s(m)p_z(l)\| + \|s(m)p_x(l)\| + \|p_z(m)p_z(l)\| + \|p_z(m)p_x(l)\| + \|p_x(m)p_x(l)\|$	11.6923
	$\|s(m)s(l)\| + \|s(m)p_z(l)\| + \|s(m)p_y(l)\| + \|p_z(m)p_z(l)\| + \|p_z(m)p_y(l)\| + \|p_y(m)p_y(l)\|$	17.6483
	$\|s(m)s(l)\| + \|s(m)p_x(l)\| + \|s(m)p_y(l)\| + \|p_x(m)p_x(l)\| + \|p_x(m)p_y(l)\| + \|p_y(m)p_y(l)\|$	19.2212
BCO-C_{16} Bond-3	$\|s(m)s(l)\| + \|s(m)p_z(l)\| + \|s(m)p_x(l)\| + \|p_z(m)p_z(l)\| + \|p_z(m)p_x(l)\| + \|p_x(m)p_x(l)\|$	20.8772
	$\|s(m)s(l)\| + \|s(m)p_x(l)\| + \|s(m)p_y(l)\| + \|p_x(m)p_x(l)\| + \|p_x(m)p_y(l)\| + \|p_y(m)p_y(l)\|$	21.3259
Graphene	$\|s(m)s(l)\| + \|s(m)p_x(l)\| + \|s(m)p_y(l)\| + \|p_x(m)p_x(l)\| + \|p_x(m)p_y(l)\| + \|p_y(m)p_y(l)\|$	22.5122
sp^3 bonds	Sum forms for the absolute values of interatomic matrix elements of sp^3 in Table I	Value (eV)
T-carbon Bond-1	$\|s(m)s(l)\| + \|s(m)p_z(l)\| + \|s(m)p_x(l)\| + \|s(m)p_y(l)\|$ $+\|p_z(m)p_z(l)\| + \|p_z(m)p_x(l)\| + \|p_z(m)p_y(l)\| + \|p_x(m)p_y(l)\| + \|p_y(m)p_y(l)\|$	21.4032
T-carbon Bond-2	$\|s(m)s(l)\| + \|s(m)p_z(l)\| + \|s(m)p_x(l)\| + \|s(m)p_y(l)\|$ $+\|p_z(m)p_z(l)\| + \|p_z(m)p_x(l)\| + \|p_z(m)p_y(l)\| + \|p_x(m)p_y(l)\| + \|p_y(m)p_y(l)\|$	20.4579
Diamond	$\|s(m)s(l)\| + \|s(m)p_z(l)\| + \|s(m)p_x(l)\| + \|s(m)p_y(l)\|$ $+\|p_z(m)p_z(l)\| + \|p_z(m)p_x(l)\| + \|p_z(m)p_y(l)\| + \|p_x(m)p_y(l)\| + \|p_y(m)p_y(l)\|$	22.5012

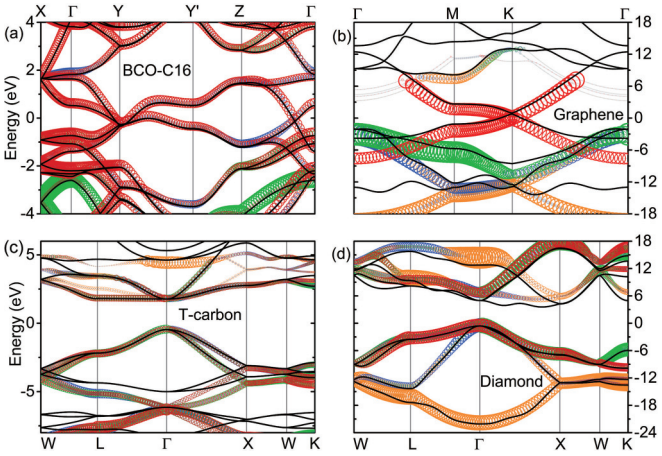

FIG. 3. Electronic band structures of (a) BCO-C_{16}, (b) graphene, (c) T-carbon, and (d) diamond. The size of the orange, blue, green, and red circles represents the proportions of the orbital s, p_x, p_y, and p_z, respectively. The black solid lines are the band structures from *ab initio* tight-binding calculations by applying Wannier90.

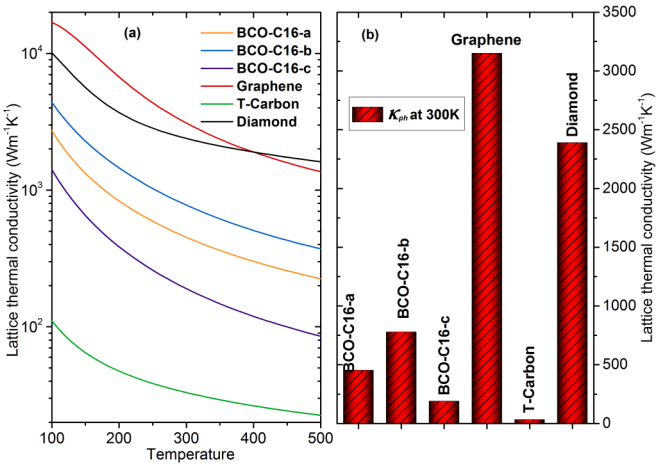

FIG. 4. (a) Temperature dependent lattice thermal conductivity of the four carbon allotropes. The orange, blue, purple, red, green, and black line represents the results for BCO-$C_{16}(\vec{a},\vec{b},\vec{c})$, graphene, T-carbon, and diamond, respectively. (b) Comparison of the lattice thermal conductivity between BCO-$C_{16}(\vec{a},\vec{b},\vec{c})$, graphene, T-carbon, and diamond at 300 K.

C. Thermal conductivity

1. Results from BTE

We shall invoke the phonon Boltzmann transport equation (BTE) to study the thermal transport properties of the systems under investigation. The lattice thermal conductivity tensor (κ) can be expressed as [19]

$$\kappa = \sum_p \sum_q C_{\rm ph} v_g(p,q)^2 \tau(p,q), \qquad (1)$$

where p and q denote the phonon branch and wave vector, respectively, $v_g = d\omega/dk$ is the phonon group velocity, τ is the phonon lifetime, and $C_{\rm ph}$ is the specific heat capacity of phonons [19,20]. The harmonic (second order) interatomic force constants (IFCs) were obtained within the linear response framework by employing the density functional perturbation theory (DFPT) as implemented in the VASP package [11,12]. Then we obtained the phonon dispersion using the PHONOPY package [16] based on the harmonic IFCs, as shown in Fig. 2. From phonon dispersions we can obtain $C_{\rm ph}$ and v_g. For the calculation of κ, anharmonic (third order) IFCs are also required. The same supercell and k mesh were used to get the third order IFCs, and the interactions between atoms were taken into account up to sixth nearest neighbors. With the third order IFCs, we solved the phonon BTE with iterative method as implemented in ShengBTE package [21]. We also calculated the scattering rate of each phonon mode $1/\tau(p,q)$. The phonon-isotope scattering process is included in all our BTE calculations. The grid convergence in k space and the force cutoff distance of all cases were examined and all the κ reported here are the final converged values. In addition, the thickness of 2D graphene is taken as 3.4 Å.

In Fig. 4(a) we present the temperature dependent κ of four carbon allotropes. The κ at 300 K are compared in Fig. 4(b), from which we see that the thermal conductivity of BCO-C_{16} has strong anisotropy. This feature is significant to the design of devices in terms of thermal management. The κ of BCO-C_{16} along three directions of the vectors of the primitive cell are $\kappa(\vec{a}) = 452.47$ W/mK, $\kappa(\vec{b}) = 777.68$ W/mK, and $\kappa(\vec{c}) = 190.18$ W/mK, respectively. The highest value is about four times larger than the lowest one. However, all of the three κ values are much lower than that for graphene (3151.53 W/mK, which is comparable to the previous work [20]). Despite the same sp^3 hybridization, T-carbon possesses the lowest κ (33.06 W/mK) among the four carbon allotropes, which is almost two orders of magnitude lower than that for diamond (κ = 2388.69 W/mK, which is in good agreement with the experimental value of natural diamond (about 2200 W/mK) [22]).

2. Bond strength

To analyze the thermal conductivity behavior of the four allotropes with sp^2 and sp^3 hybrid, we calculated the atomic potential energy with respect to bond length for each allotrope. In the unit cell of each allotrope, only one single bond changes, while keeping all other bonds unchanged. From the geometrical symmetry we can learn that there only exist two kinds of atomic bonds in T-carbon and three kinds of atomic bonds in BCO-C_{16}, which are labeled in Fig. 5. The results are shown in Fig. 5. To identify the bond strength, we applied the second order polynomial (parabolic) fitting to the potential energy versus the bond length. Then the coefficients of the second order fitting (spring constant) can indicate the bond strength. The data are collected in Table III. From Fig. 5 and Table III we can see that (1) the spring constants of three kinds of bonds in BOC-C_{16} are almost the same, (2) the bond spring constant of graphene is about four times larger than that of BCO-C_{16} bonds, (3) for T-carbon the spring constant of bond-1 is about ~1.34 times of that for bond-2, and (4) the bond strength of diamond is about 1.9–2.6 times of the bond strength in T-carbon. These results are consistent with the atomic orbital bonding in Table II.

From Fig. 5 and Table III we can also clearly see that graphene with the regular sp^2 hybridization owns a lower potential energy than BCO-C_{16} with irregular sp^2 hybridiza-

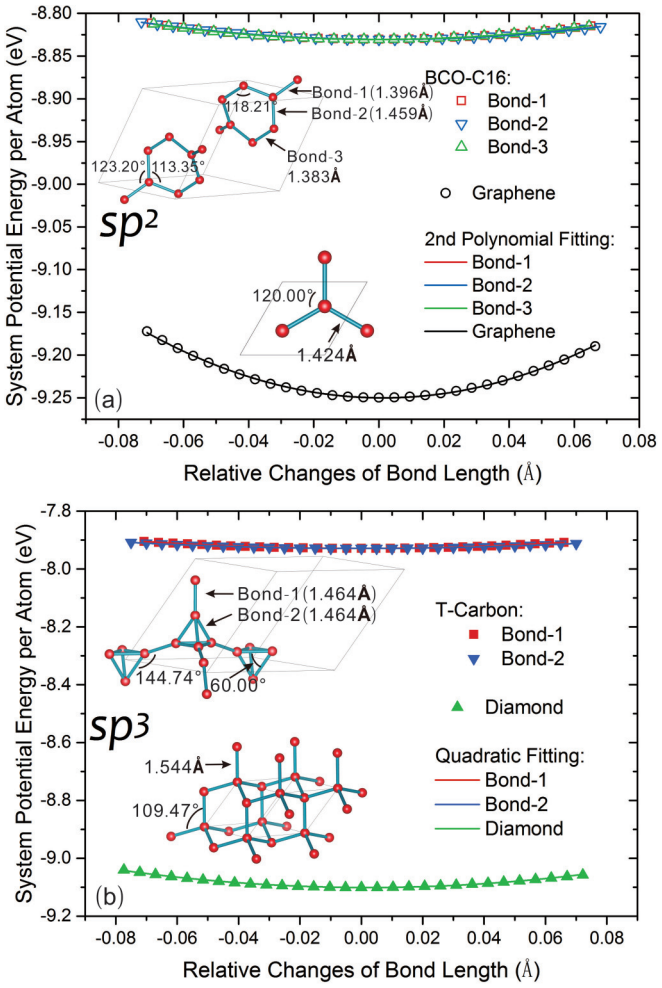

FIG. 5. (a) Atomic potential energy with respect to the relative change of the sp^2 bond length. The red open squares, blue open invert triangles, green open triangles, and black open circles represent three kinds of bonds in BCO-C_{16} and the unique bond in graphene, respectively. (b) Atomic potential energy with respect to the relative change of the sp^3 bond length. The red solid squares, blue solid invert triangles, and green solid triangles represent two kinds of bonds in T-carbon and the unique bond in diamond, respectively. The solid lines are the second order polynomial fitting to each energy curve.

tion. Meanwhile, diamond with regular sp^3 hybridization has a lower potential energy than T-carbon with irregular sp^3 hybridization. These results imply that graphene is more stable than BCO-C_{16} and diamond is more stable than T-carbon, which follows the common sense. From the information of bond spring constants we can also learn that although both BCO-C_{16} and graphene possess sp^2 hybridization, the bond strength considerably differs from each other. Analogously, diamond and T-carbon which possess the sp^3 hybridization also exhibit significantly different bond spring constants. In addition, from the κ results in Fig. 4, we can infer that the bond spring constant is a partial factor to determine the κ. The larger bond spring constant, meaning stiffer bonds, corresponds to a higher ability of thermal transport of phonons (larger κ). In addition, the effective spring constants are not simply correlated with the distance between atoms (bond length). As

TABLE III. The coefficients of the second order polynomial fitting to the atomic potential energy of sp^2 and sp^3 bonds presented in Fig. 5.

Hybridization style	Bond identity	Bond length (Å)	Second order coefficient (eV/Å^2)
sp^2	BCO-C_{16} Bond-1	1.3960	3.8021
	BCO-C_{16} Bond-2	1.4590	3.5114
	BCO-C_{16} Bond-3	1.3830	3.7452
	Graphene	1.4240	14.5226
sp^3	T-carbon Bond-1	1.4640	4.8080
	T-carbon Bond-2	1.4640	3.5788
	Diamond	1.5440	9.2569

shown in Table III, the bond strength (the effective spring constant) is also related to the form of the hybridization. This is why in T-carbon the two kinds of the C-C bonds have the same bond length, however, their effective spring constants are different. This can be further confirmed later in Fig. 7(a).

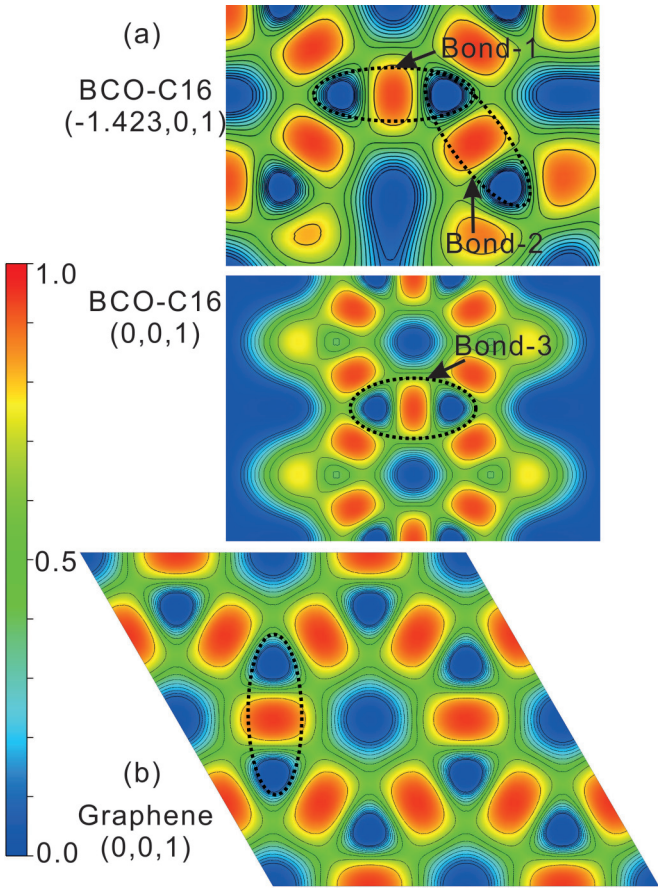

FIG. 6. (a) Electron local function (ELF) of BCO-C_{16}. The specific 2D-slice projections are chosen to show the different three bonds in BCO-C_{16}. (b) ELF of graphene. The color bar indicates the density intensity of the local electrons. The values of 0.5 and 1.0 represent fully delocalized (homogeneous electron gas) and fully localized electrons, respectively, while the value of 0.0 refers to very low charge density.

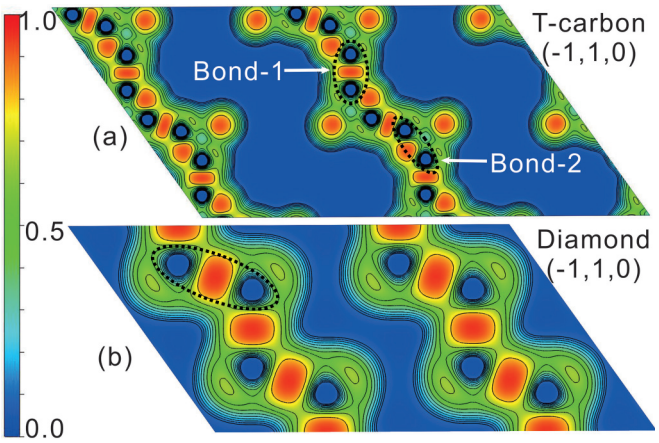

FIG. 7. (a) ELF of T-carbon. The specific 2D-slice projections are chosen to show the two different types of bonds in T-carbon. (b) ELF of diamond.

3. *Electronic structure and anharmonicity of bonds*

From Eq. (1) we know that another important factor to determine κ is phonon lifetime (τ), which corresponds to the phonon scattering process and is related to the anharmonicity of the interactions among the atoms. To characterize the anharmonicity of bonds, first we calculate the electron local function (ELF) [23] of each allotrope to present the electronic structure of the sp^2 and sp^3 bonds, which is based on the jellium electron gas model and its value is normalized between 0.0 and 1.0. The value of 0.5 and 1.0 represents fully delocalized (homogeneous electron gas) and fully localized electrons, respectively, while the value of 0.0 refers to very low charge density. The ELF results are shown in Figs. 6 and 7. From Fig. 6 the covalent bonds of the sp^2 hybrid are clearly seen. Although the ELF of these sp^2 bonds looks the same, from the contour lines we can still see that the bond-2 in BCO-C_{16} is a little bit different from the other two bonds (bond-1 and bond-3) in the same structure, and is also different from the bond in graphene. The ELF of bond-2 is not axisymmetric along the bond direction. The result is consistent with the TB calculations in Table I. From Fig. 7 it is clearly observed that the bond-1 in T-carbon is similar with the bond of diamond. However, the bond-2 shows very different distribution as compared to the normal sp^3 bond in diamond. This result is also consistent with the data in Table I. The ELF in Figs. 6 and 7 reflect the different bonding styles determined by the structures of each allotrope.

To further study the anharmonicity of the sp^2 and sp^3 bonds in these carbon allotropes, we use a method named the regular residual analysis we proposed recently [24]. First, we calculate the atomic potential energy curve with respect to bond length of each allotrope and then perform the second polynomial fittings which are presented in Fig. 5. It is worth pointing out that for the fitting process we adopt the least-squares algorithm in common sense, as implemented in the graph software OriginPro 9.0.0. We take the same quadratic fitting procedure for all curves. The fittings show robustness and the fixed fitting procedure will not affect the residual behavior. Here the regular residual r_i is defined as the difference between the observed values and the predicted values of the second polynomial

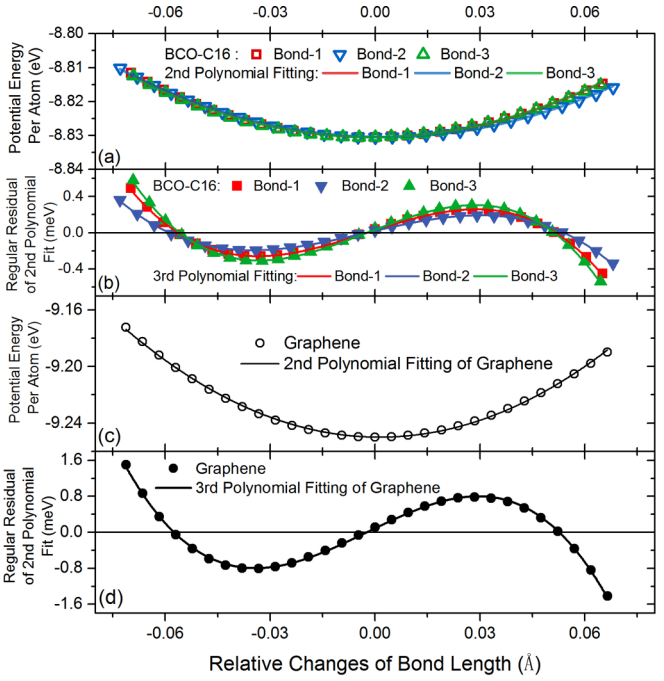

FIG. 8. Atomic potential energy with respect to the bond length of sp^2 bonds of (a) BCO-C_{16} and (c) graphene, respectively. The solid color lines represent the second polynomial fittings. (b) and (d) Regular residuals from the second polynomial fittings to (a) and (c), respectively, and the solid lines are the third polynomial fittings.

fittings. Then, the r_i can describe the anharmonicity of the potential energy curves. To determine the value of the perturbations, we first run equilibrium *ab initio* molecular dynamics (EAIMD) simulations of each allotrope with *NVT* (constant particles, volume, and temperature) ensemble at 300 K with 10 ps, during which we record the amplitude of the vibration of each atom and then take the average value as the effective amplitude of the atomic vibrations. We then use this value as the maximum displacement in analyzing the residuals. The related regular residuals for sp^2 and sp^3 bonds are presented in Figs. 8 and 9. From Figs. 8(b) and 8(d) we can learn that all the residuals for the sp^2 bonds show the third polynomial function behavior very well, as all the residuals are in the level of "meV". In Figs. 9(c) and 9(e) we can see that the residuals of the bond-2 (intratetrahedron) in T-carbon and the bond in diamond also show well the third polynomial function behavior, however, the residuals for bond-1 (intertetrahedron) in T-carbon shows the fourth polynomial function behavior in Fig. 9(b), which means the fourth order anharmonicity is strong in T-carbon compared with the third anharmonicity term and cannot be ignored.

To compare the anharmonicity of the sp^2 and sp^3 bonds, here we calculated the relative regular residuals through dividing the residuals by the corresponding potential-well depth values. It is natural to find that a larger potential well can own the relative larger residuals. The phonon scattering rate from anharmonicity depends on both harmonic and anharmonic IFCs [25]. It makes no sense by only characterizing the amplitude of the anharmonic IFCs to estimate the degree of anharmonicity in materials [25]. In order to estimate the

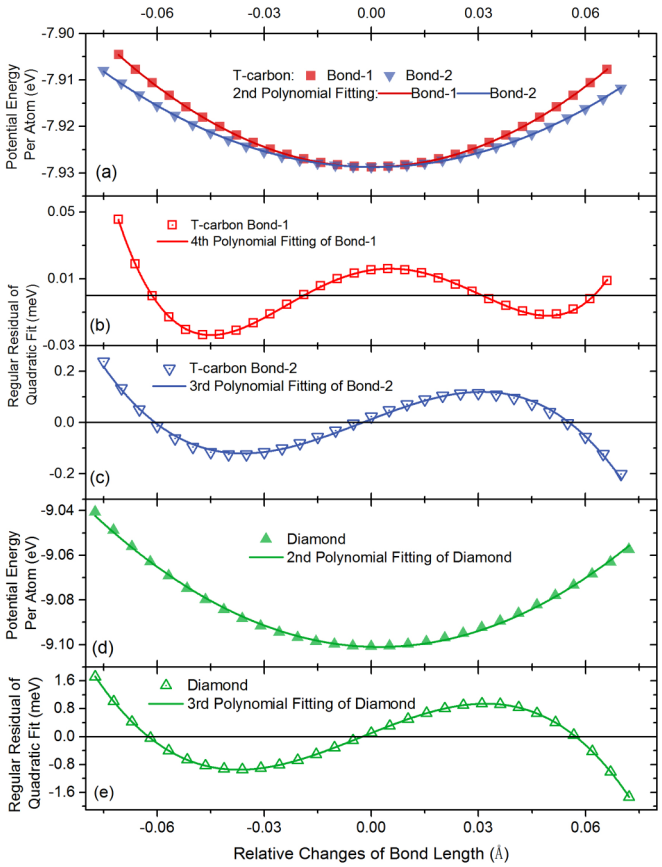

FIG. 9. Atomic potential energy with respect to the bond length of sp^3 bonds of (a) T-carbon and (d) diamond, respectively. The solid lines represent the second polynomial fittings. (b), (c), and (e) Regular residuals from the second polynomial fittings in (a) and (d), respectively. In (b), the solid red line is the fourth polynomial fitting and in (c) and (e) the blue and green solid lines represent the third polynomial fittings.

anharmonicity of the atomic bonds more objectively, we adopt the relative regular residuals here. The results are presented in Fig. 10. The relative residuals can indicate the anharmonicity of the related bonds intuitively. From Fig. 10(a) we can learn that the anharmonicity along the sp^2 bonds is almost the same for graphene and BCO-C_{16}. In particular, the graphene and bond-2 in BCO-C_{16} possess relatively the smallest anharmonicity. In Fig. 10(b) we see that in the direction along the sp^3 bonds, the bond-2 in T-carbon has an anharmonicity similar to diamond. Although the residual of bond-1 in T-carbon shows the strong fourth order polynomial behavior, the relative residual value is smaller than those of other sp^3 bonds, which corresponds to small anharmonicity in bond-1 along the bond direction. In addition, the relative residuals of bond-1 and bond-2 of T-carbon are around 3% and 1/3 of the diamond, respectively.

It is worth pointing out that all the phonon interactions are carried by the atomic bonds, and all the complex displacement of phonons in space can be projected on the two directions: along and perpendicular to the atomic bonds. By performing the similar calculations above, we also calculated the atomic potential energy curves versus the displacement

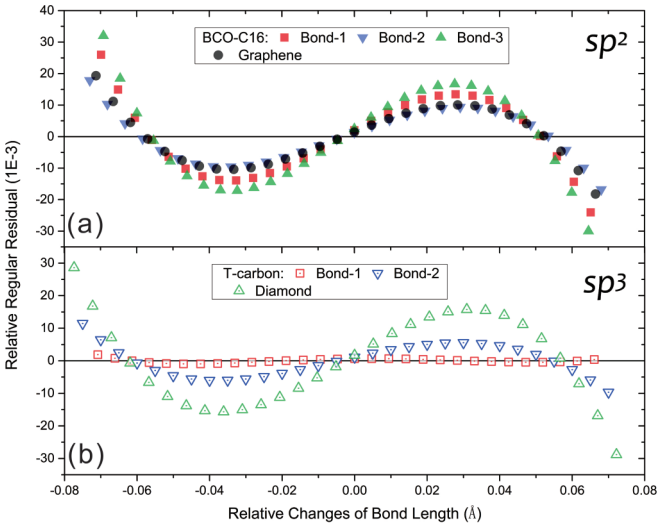

FIG. 10. The relative regular residuals of the second polynomial fittings to the potential energy with respect to the bonds length of sp^2 graphene (a) and sp^3 diamond (b).

perpendicular to the sp^2 and sp^3 bonds, which are presented in Figs. 11(a)–11(d). In BCO-C_{16} there are two nonequivalent kinds of atoms, and for the other three allotropes there is only one unique kind of atom. The direction of displacement perpendicular to the sp^2 and sp^3 bonds are illustrated in Figs. 11(a)–11(d). The relative regular residuals corresponding to each second polynomial fitting are also calculated and presented in Figs. 11(e) and 11(f), from which we observe that in the direction perpendicular to the sp^2 bonds, the relative residuals of atom-1 and atom-2 in BCO-C_{16} are similar and much larger than the relative residuals of graphene. For the displacement perpendicular to the sp^3 bonds, the relative residual in T-carbon is much larger than diamond. The above results imply that when the displacement is perpendicular to the sp^2 and sp^3 bonds, graphene and diamond have smaller anharmonicity than BCO-C_{16} and T-carbon. Thus, we might infer the anharmonicity of atomic bonds by combining with the information in Fig. 10. From Figs. 10(a) and 11(e) it is easily seen that graphene owns smaller anharmonicity of atomic bonds than BCO-C_{16}. In Fig. 11(f) the relative residuals of diamond are only 1% of T-carbon for the displacement perpendicular to the bond direction. Although in Fig. 10(b) the relative residuals of bond-1 and bond-2 in T-carbon are around 3% and 1/3 of the diamond, respectively, we can still infer that the diamond possesses anharmonicity of atomic bonds smaller than T-carbon.

Now, by combining with the information in Table I, we find that the standard sp^2 and sp^3 hybridizations possess relatively smaller anharmonicity in atomic bonds. From electron local function in space shown in Figs. 6 and 7, we observe that the standard sp^2 and sp^3 hybridizations have the most symmetrical charge distribution in space. Since the charge distribution also determines the interatomic interactions (e.g., force constants), we infer that this may be the reason that leads to different anharmonicities in atomic bonds. From Tables II and III we notice that the standard sp^2 and sp^3 hybridizations correspond to stronger atomic bonding strength than that in novel sp^2 and sp^3 hybridizations. All these analyses are consistent with the results of κ in Fig. 4.

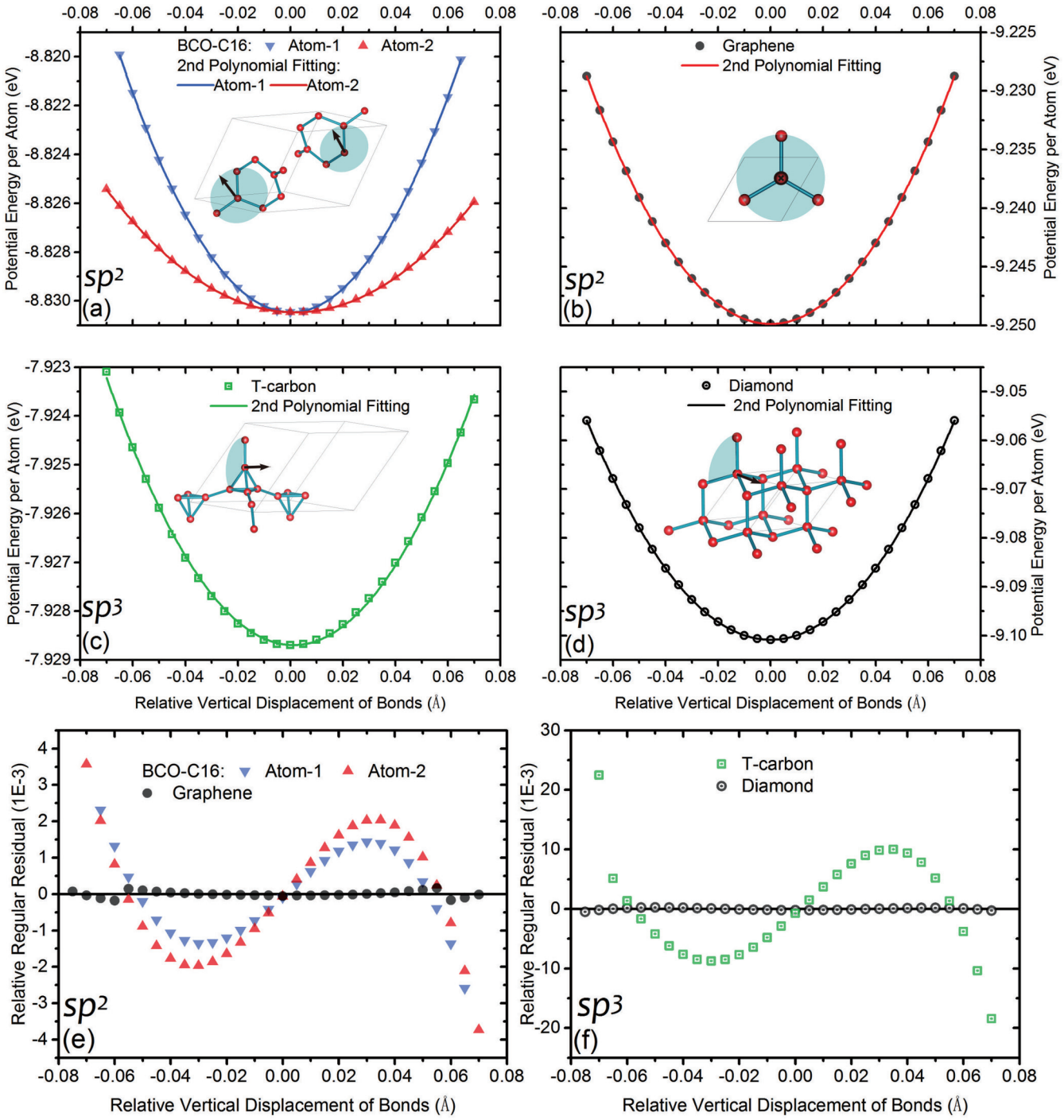

FIG. 11. Atomic potential energy with respect to the displacement perpendicular to the sp^2 and sp^3 bonds. The red solid triangle, blue solid invert triangles, and black solid circles represent the two nonequivalent kinds of atoms in BCO-C_{16} (a) and a unique kind of atom in graphene (b). The green open squares and black open circles represent the unique kind of atom in (c) T-carbon and (d) diamond. The corresponding color solid lines in (a)–(d) are the second order polynomial fitting of each energy curve. All the directions of the displacements are illustrated in (a)–(d). (e) and (f) The relative regular residuals of the second polynomial fittings for the potential energy with respect to the displacement perpendicular to the sp^2 and sp^3 bonds.

4. Phonon anharmonicity

From Eq. (1) we know that κ relies on the phonon heat capacity $C_{\rm ph}$, the phonon group velocity v_g, and the phonon scattering lifetime τ. From the phonon BTE calculations with ShengBTE package [21,26,27] based on *ab initio*, we obtained the three key parameters $C_{\rm ph}$, v_g, and τ of each allotrope. The details of the $C_{\rm ph}$, v_g, and τ can be found in the Supplemental Material [17]. In addition, through the analysis of these three key parameters, we can learn that (1) the $C_{\rm ph}$ of four allotropes are approximately the same; (2) the anisotropy

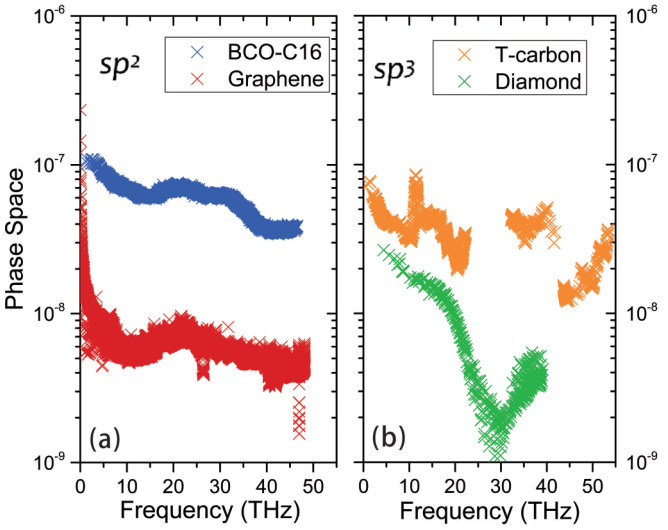

FIG. 12. Frequency dependence of three-phonon scattering phase space at 300 K for all three-phonon processes of carbon allotropes with sp^2 (a) and sp^3 (b) hybrid.

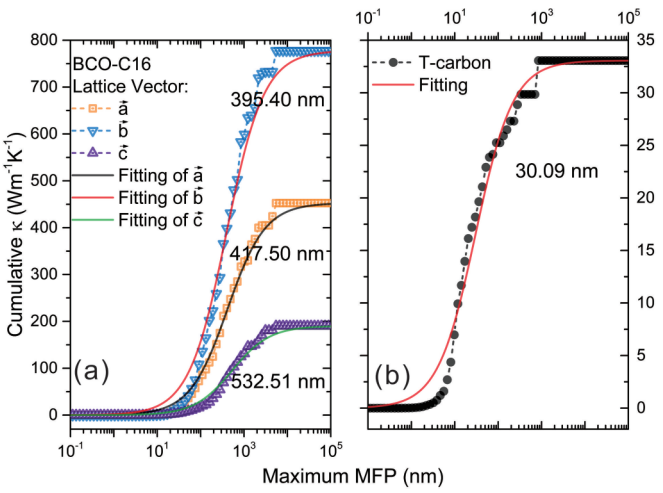

FIG. 13. Accumulative lattice thermal conductivity of (a) BCO-C_{16} and (b) T-carbon as a function of phonon mean free path at 300 K. The solid lines are fitting to the results.

of the v_g along the three lattice vectors of BCO-C_{16} leads to the different κ in three directions; (3) although there exist the difference among the group velocity of the carbon allotropes, the amplitudes of v_g from these allotropes are in the same level; and (4) τ is the dominant parameter determining κ in the three components.

To investigate the phonon scattering mechanism more deeply, we calculate the allowed phase space for three-phonon processes P_3 [21,28]. At 300 K, where three-phonon processes are dominant, the total phase space for three-phonon processes is defined by

$$P_3 = \frac{2}{3\Omega}\left(\sum_j \int D_j^{(+)}(q)dq + \frac{1}{2}\sum_j \int D_j^{(-)}(q)dq\right),$$

where Ω is a normalization factor, j index the phonon branches, q is the wave vector, and

$$D_j^{(\pm)}(q) = \sum_{j',j''} \int \delta[\omega_j(q) \pm \omega_{j'}(q') - \omega_{j''}(q \pm q'' - G)]dq',$$

where $D_j^{(+)}(q)$ corresponds to absorption processes, i.e., $\omega_j(q) + \omega_{j'}(q') = \omega_{j''}(q + q'' - G)$, whereas $D_j^{(-)}(q)$ corresponds to emission processes, i.e., $\omega_j(q) = \omega_{j'}(q') + \omega_{j''}(q - q'' - G)$. P_3 contains a large amount of scattering events that satisfy the conservation conditions and can be used to assess quantitatively the number of scattering channels available for each phonon mode. Less restricted phase space for three-phonon processes implies a larger number of available scattering channels. Consequently, there is an inverse relationship between P_3 and the intrinsic lattice thermal conductivity of a material [28,29]. From Figs. 12(a) and 12(b) we can find that graphene owns smaller P_3 phase values than BCO-C_{16} and the P_3 values of diamond is smaller than T-carbon. The result is consistent with the κ and anharmonicity properties we discuss above. In addition, we also calculate the Grüneisen parameter $\gamma_j(q)$ with $\gamma_j(q) = -\frac{a_0}{\omega_j(q)}\frac{\partial\omega_j(q)}{\partial a}$, where a_0 is the equilibrium lattice constant, j is phonon branch index, and q is wave vector. The Grüneisen parameter of each allotrope and related analysis can be found in the Supplemental Material [17].

Since the phonon thermal conductivity can be modulated through nanostructuring in practical design of nanodevices, we investigate the size dependence of κ for the novel carbon allotropes at 300 K by calculating the accumulative thermal conductivity with respect to the maximum mean-free path (MFP) allowed. The accumulative κ are plotted in Fig. 13. The accumulated κ increases with MFP increasing, until it reaches the limit above a length which represents the longest MFP of the heat carriers. In order to characterize the critical MFP, we can fit the accumulative κ with a uniparametric function [21]

$$\kappa(l \leqslant l_{\max}) = \frac{\kappa_{\max}}{1 + \frac{l_0}{l_{\max}}},$$

where $\kappa_{\max}$ is the ultimate accumulative thermal conductivity, $l_{\max}$ is the maximal MFP concerned, and l_0 is the parameter to be evaluated. The fitted curves at 300 K are plotted in Fig. 13. The yielded parameters l_0 of BCO-C_{16} along the three lattice vectors are 417.50, 395.40, and 532.51 nm, respectively, which again shows the strong anisotropy. There is an interesting and abnormal phenomenon in Fig. 13(a) that the smaller κ corresponds to a larger critical MFP l_0. Normally the larger κ corresponds to the longer l_0. The l_0 of T-carbon is 30.09 nm. The effective MFP in Fig. 13 is significant to the nanodevice design when involving these carbon allotropes.

IV. CONCLUSION

In summary, from the perspective of orbital hybridization, interatomic covalent bonds, and phonons, we systematically studied the thermal transport properties of two novel carbon allotropes with sp^2 (BCO-C_{16}) and sp^3 (T-carbon) hybridization, respectively. For comparison, graphene and diamond with standard sp^2 and sp^3 hybridization, respectively, are also studied. We first calculate the hybrid orbitals with the tight-binding method to pinpoint the difference in the covalent bonds

between the sp^2 BCO-C_{16} and the standard sp^2 graphene, and between the sp^3 T-carbon and diamond. Next, we implement the phonon Boltzmann transport equation to evaluate the lattice thermal conductivity of each allotrope. The lattice thermal conductivity exhibits large diversity, despite the similar bonding nature. To explore the underlying mechanism, we calculate the bond spring constant to investigate the strength of the related covalent bonds, with the electron local functions showing the forms of the covalent bonds. We also implement our newly developed residual analysis method to qualitatively characterize the anharmonicity of the covalent bonds. We found that the allotropes with standard sp^2 (graphene) and sp^3 (diamond) atomic orbital hybridization own stronger atomic bonding strength and smaller anharmonicity than the allotropes with novel sp^2 (BCO-C_{16}) and sp^3 (T-carbon) hybridization. Such a conclusion is further confirmed by the mode level analysis of heat capacity, group velocity, and phonon lifetime for each allotrope within the framework of the phonon Boltzmann transport equation. We expect that the method of analyzing phonon anharmonicity from orbital hybridization could pave the way for better understanding the thermal transport process in crystalline materials.

ACKNOWLEDGMENTS

S.-Y.Y. gratefully thanks Dr. Simin Nie (Stanford University) for providing the structure of BCO-C_{16}. The authors gratefully acknowledge the computing time granted by the John von Neumann Institute for Computing (NIC) and provided on the supercomputer JURECA at Jülich Supercomputing Centre (JSC) (Project No. JHPC25) and the Jülich Aachen Research Alliance-High Performance Computing (JARA-HPC) from (RWTH Aachen University under Project No. jara0145. M.H. is grateful for the financial support from the Natural National Science Foundation of China (Grant No. 51528203). G.S. is supported in part by the MOST of China (Grant No. 2013CB933401), NSFC (Grant No. 14474279), and the Strategic Priority Research Program of the Chinese Academy of Sciences (Grant No. XDB07010100).

S.-Y.Y. and G.Q. contributed equally to this work.

[1] K. S. Novoselov, A. K. Geim, S. V. Morozov, D. Jiang, M. I. Katsnelson, I. V. Grigorieva, S. V. Dubonos, and A. A. Firsov, Nature (London) **438**, 197 (2005).

[2] M. H. Nazaré and A. J. Neves, *Properties, Growth and Applications of Diamond* (INSPEC, The Institution of Electrical Engineers, London, 2001).

[3] H. W. Kroto, J. R. Heath, S. C. O'Brien, R. F. Curl, and R. E. Smalley, Nature (London) **318**, 162 (1985).

[4] S. Iijima, Nature (London) **354**, 56 (1991).

[5] K. S. Novoselov, A. K. Geim, S. V. Morozov, D. Jiang, Y. Zhang, S. V. Dubonos, I. V. Grigorieva, and A. A. Firsov, Science **306**, 666 (2004).

[6] J.-T. Wang, H. Weng, S. Nie, Z. Fang, Y. Kawazoe, and C. Chen, Phys. Rev. Lett. **116**, 195501 (2016).

[7] X.-L. Sheng, Q.-B. Yan, F. Ye, Q.-R. Zheng, and G. Su, Phys. Rev. Lett. **106**, 155703 (2011).

[8] N. Marzari and D. Vanderbilt, Phys. Rev. B **56**, 12847 (1997).

[9] I. Souza, N. Marzari, and D. Vanderbilt, Phys. Rev. B **65**, 035109 (2001).

[10] A. A. Mostofi, J. R. Yates, G. Pizzi, Y.-S. Lee, I. Souza, D. Vanderbilt, and N. Marzari, Comput. Phys. Commun. **185**, 2309 (2014).

[11] G. Kresse and J. Furthmüller, Phys. Rev. B **54**, 11169 (1996).

[12] G. Kresse and J. Furthmüller, Comput. Mater. Sci. **6**, 15 (1996).

[13] P. E. Blöchl, Phys. Rev. B **50**, 17953 (1994).

[14] G. Kresse and D. Joubert, Phys. Rev. B **59**, 1758 (1999).

[15] J. P. Perdew, K. Burke, and M. Ernzerhof, Phys. Rev. Lett. **77**, 3865 (1996).

[16] A. Togo and I. Tanaka, Scr. Mater. **108**, 1 (2015).

[17] See Supplemental Material at http://link.aps.org/supplemental/10.1103/PhysRevB.95.085207 for the details of analytical expression of the hybrid orbitals of four carbon allotropes and the properties of phonons from BTE calculations.

[18] R. Andrievski, Int. J. Refract. Metals Hard Mater. **19**, 447 (2001).

[19] J. E. Turney, E. S. Landry, A. J. H. McGaughey, and C. H. Amon, Phys. Rev. B **79**, 064301 (2009).

[20] S.-Y. Yue, T. Ouyang, and M. Hu, Sci. Rep. **5**, 15440 (2015).

[21] W. Li, J. Carrete, N. A. Katcho, and N. Mingo, Comput. Phys. Commun. **185**, 1747 (2014).

[22] K. Plamann and D. Fournier, Phys. Status Solidi A **154**, 351 (1996).

[23] B. Silvi and A. Savin, Nature (London) **371**, 683 (1994).

[24] S.-Y. Yue, X. Zhang, G. Qin, S. Phillpot, and M. Hu, A Metric for Strong Intrinsic Fourth-Order Phonon Anharmonicity (unpublished).

[25] L. Lindsay, D. A. Broido, and T. L. Reinecke, Phys. Rev. B **87**, 165201 (2013).

[26] W. Li, N. Mingo, L. Lindsay, D. A. Broido, D. A. Stewart, and N. A. Katcho, Phys. Rev. B **85**, 195436 (2012).

[27] W. Li, L. Lindsay, D. A. Broido, D. A. Stewart, and N. Mingo, Phys. Rev. B **86**, 174307 (2012).

[28] L. Lindsay and D. A. Broido, J. Phys. Condens. Matter **20**, 165209 (2008).

[29] J. M. Ziman, *Electrons and Phonons: The Theory of Transport Phenomena in Solids* (Oxford University Press, Oxford, 1960).